

# Synthesis of $\beta$ -Mg<sub>2</sub>C<sub>3</sub>: A Monoclinic High-Pressure Polymorph of Magnesium Sesquicarbide

Timothy A. Strobel,<sup>\*,†</sup> Oleksandr O. Kurakevych,<sup>†,‡</sup> Duck Young Kim,<sup>†</sup> Yann Le Godec,<sup>‡</sup> Wilson Crichton,<sup>§</sup> Jérémy Guignard,<sup>§</sup> Nicolas Guignot,<sup>||</sup> George D. Cody,<sup>†</sup> and Artem R. Oganov<sup>⊥,#,∇,○</sup>

<sup>†</sup>Geophysical Laboratory, Carnegie Institution of Washington, 5251 Broad Branch Road Northwest, Washington, D.C. 20015, United States

<sup>‡</sup>IMPMC, UPMC Sorbonne Universités, UMR CNRS 7590, Muséum National d'Histoire Naturelle, IRD UMR 206, Paris 75005, France

<sup>§</sup>European Synchrotron Radiation Facility, 71, Avenue des Martyrs, Grenoble 38043, France

<sup>||</sup>Synchrotron SOLEIL, L'Orme des Merisiers Saint-Aubin, Gif-sur-Yvette 91192, France

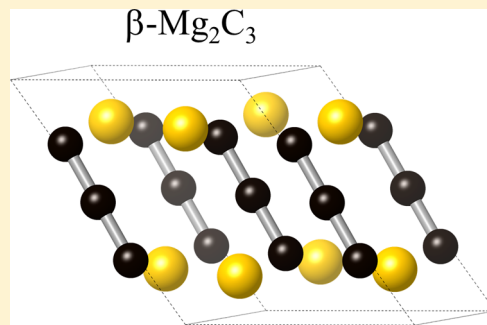
<sup>⊥</sup>Department of Geosciences, State University of New York, Stony Brook, New York 11794-2100, United States

<sup>#</sup>Center for Materials by Design, Institute for Advanced Computational Science, State University of New York, Stony Brook, New York 11794-2100, United States

<sup>∇</sup>Moscow Institute of Physics and Technology, 9 Institutskiy Lane, Dolgoprudny City, Moscow Region 141700, Russian Federation

<sup>○</sup>Northwestern Polytechnical University, Xi'an 710072, China

**ABSTRACT:** A new monoclinic variation of Mg<sub>2</sub>C<sub>3</sub> was synthesized from the elements under high-pressure (HP), high-temperature (HT) conditions. Formation of the new compound, which can be recovered to ambient conditions, was observed *in situ* using X-ray diffraction with synchrotron radiation. The structural solution was achieved by utilizing accurate theoretical results obtained from *ab initio* evolutionary structure prediction algorithm USPEX. Like the previously known orthorhombic *Pnmm* structure ( $\alpha$ -Mg<sub>2</sub>C<sub>3</sub>), the new monoclinic *C2/m* structure ( $\beta$ -Mg<sub>2</sub>C<sub>3</sub>) contains linear C<sub>3</sub><sup>4-</sup> chains that are isoelectronic with CO<sub>2</sub>. Unlike  $\alpha$ -Mg<sub>2</sub>C<sub>3</sub>, which contains alternating layers of C<sub>3</sub><sup>4-</sup> chains oriented in opposite directions, all C<sub>3</sub><sup>4-</sup> chains within  $\beta$ -Mg<sub>2</sub>C<sub>3</sub> are nearly aligned along the crystallographic *c*-axis. Hydrolysis of  $\beta$ -Mg<sub>2</sub>C<sub>3</sub> yields C<sub>3</sub>H<sub>4</sub>, as detected by mass spectrometry, while Raman and NMR measurements show clear C=C stretching near 1200 cm<sup>-1</sup> and <sup>13</sup>C resonances confirming the presence of the rare allenide anion.



## INTRODUCTION

Alkali and alkaline earth metal carbides may be generally classified into three categories based on carbon bonding motifs.<sup>1</sup> The most common carbides (acetylides) contain carbon dumbbell pairs (C<sub>2</sub><sup>2-</sup>), such as those found in CaC<sub>2</sub> or Li<sub>2</sub>C<sub>2</sub>.<sup>2,3</sup> These are followed by less common methanide (e.g., Be<sub>2</sub>C)<sup>4</sup> and allenide (e.g., Mg<sub>2</sub>C<sub>3</sub><sup>5</sup> and nonalkali/alkaline earth Sc<sub>3</sub>C<sub>4</sub><sup>6,7</sup>) type carbides, which contain isolated single carbon anions (C<sup>4-</sup>) and three carbon chains (C<sub>3</sub><sup>4-</sup>), respectively. Magnesium carbides are unique in the sense that all three carbon bonding motifs have been successfully prepared.<sup>5,8,9</sup>

MgC<sub>2</sub> was originally prepared by Novák in 1910 by the reaction of magnesium and acetylene.<sup>10</sup> Above 770 K, MgC<sub>2</sub> transforms into Mg<sub>2</sub>C<sub>3</sub>, and above 970 K, Mg<sub>2</sub>C<sub>3</sub> decomposes into Mg and amorphous carbon.<sup>10</sup> Both carbides are thermodynamically metastable with respect to their formation elements:  $\Delta H_f^\circ = +79.5$  kJ/mol and +87.86 kJ/mol for Mg<sub>2</sub>C<sub>3</sub> and MgC<sub>2</sub>, respectively.<sup>11</sup> The structural units within these

carbides were originally deduced from hydrolysis measurements, which either yielded acetylene or propadiene (or propyne) depending on the carbon anions present.<sup>12–16</sup> Only later were definitive structural solutions possible confirming the nature of the carbon within,<sup>5,8,17</sup> likely a result of the intrinsic metastability and reactivity of these compounds. Fjellvåg and Karen reported the structural characterization of Mg<sub>2</sub>C<sub>3</sub> in 1992, as obtained from neutron diffraction measurements on relatively pure samples.<sup>5</sup> The *Pnmm* structure contains C<sub>3</sub><sup>4-</sup> units with C=C bond lengths of 1.33 Å that are slightly enhanced through  $\pi$ -interaction with Mg. Recently, we reported the formation of Mg<sub>2</sub>C, a methanide-type carbide that contains C<sup>4-</sup> anions.<sup>9</sup>

Magnesium carbides are interesting compounds from both fundamental and applied perspectives. In the terms of searching for new advanced materials, the Mg–C system looks very

Received: April 25, 2014

Published: June 13, 2014

promising (1D polymerized carbon chains,<sup>18</sup> Mg-intercalated graphite, carbon clathrates,<sup>19</sup> etc.). However, at ambient pressure no reaction between elemental Mg and C is favorable at any temperature. The recent synthesis of Mg<sub>2</sub>C,<sup>9</sup> predicted 20 years before,<sup>20</sup> demonstrates the possibility for direct formation from the elements under high-pressure conditions ( $p > 15$  GPa,  $T \sim 1770$  K).<sup>21</sup> Two factors contribute to this simultaneously: (1) HP increases the affinity between carbon and magnesium, and (2) HP stabilizes the sp<sup>3</sup> carbon state, covalent<sup>22</sup> as well as ionic,<sup>9</sup> allowing us to consider high pressure as a powerful tool to explore magnesium–carbon chemistry and to discover new compounds with unusual bonding states and properties. In the present Article we report the synthesis of monoclinic  $\beta$ -Mg<sub>2</sub>C<sub>3</sub>, a high-pressure polymorph of magnesium sesquicarbide, previously only known as an orthorhombic ( $\alpha$ ) phase. Its monoclinic crystal structure was solved with assistance from *ab initio* evolutionary structure predictions.

## METHODS

**Sample Preparation.** All samples started with mixtures of hcp Mg (Sigma-Aldrich, 99.5%, 325 mesh) and glassy carbon (gC, Sigma-Aldrich, 99.95%, 2–12  $\mu\text{m}$ ) or graphite (Sigma-Aldrich, 99.7%, < 20  $\mu\text{m}$ ), with analogous results obtained for both carbon cases. Magnesium carbon mixtures were thoroughly mixed using a porcelain mortar in molar ratios ranging  $0.33 \leq x_{\text{C}} \leq 0.93$  and dried under vacuum at 100 °C for 12 h. Most samples were prepared under an inert argon atmosphere as a precaution to avoid oxidation, although preparation in air did not significantly alter product purity.

**Multianvil (MA).** Synthesis runs for *ex situ* characterization were performed at the Geophysical Laboratory utilizing both 14/8 and 18/11 assemblies.<sup>23</sup> Mg–C mixtures were compacted into pellets and loaded into MgO capsules with graphite or rhenium heaters and a ZrO<sub>2</sub> insulating sleeve. Experiments were conducted at pressures ranging  $\sim 5$ –15 GPa and temperatures ranging  $\sim 1500$ –2000 K with reaction times of  $\sim 1$  h, after which the sample was quenched by the switching off the power and decompressed. Recovery of all samples from the MgO capsule was conducted in an inert argon atmosphere.

*In situ* runs were performed using the newly commissioned large-volume press at beamline ID06 of the ESRF (Grenoble, France). Similar preparations were made as for the *ex situ* experiments; however, boron epoxy windows were employed in the pressure transmitting media, and windows were laser cut into the Re heater to improve X-ray transmission properties. Pressure and temperature estimations were made using equations of states of Mg and MgO.<sup>24,25</sup>

**Diamond Anvil Cell (DAC).** Symmetric diamond anvil cells (DACs) equipped with  $\sim 400$   $\mu\text{m}$  culets were used to generate high pressures. A piece of Re foil was indented to a thickness of  $\sim 60$   $\mu\text{m}$ , and a  $\sim 200$   $\mu\text{m}$  hole was drilled for the sample chamber. Mg–C mixtures were pressed into  $\sim 20 \times 10$   $\mu\text{m}^2$  discs and loaded into the sample chamber, along with a ruby sphere for pressure calibration.<sup>26</sup> Neon was used as a pressure transmitting medium and also served as thermal insulation between the sample and diamonds during heating. Samples were compressed to pressures ranging  $\sim 10$ –30 GPa and heated between  $\sim 1500$  and 2000 K using the infrared laser heating (LH) system at HPCAT, sector 16, Advanced Photon Source.<sup>27</sup>

**Paris–Edinburgh (PE) Press.** The PE press at SOLEIL was also used for synthesis and *in situ* characterization of Mg<sub>2</sub>C<sub>3</sub>. Opposite anvils with standard boron-epoxy gasket (pressure medium) were employed to create high-pressure conditions.<sup>28</sup> A graphite resistive furnace allowed heating up to 1500 K under high pressure. The Mg–C mixtures were placed into a MgO capsule in order to isolate the sample from the heater. Pressure and temperature estimations were made using equations of states of Mg and MgO.<sup>24,25</sup>

**X-ray Diffraction.** Samples recovered from multianvil synthesis runs were sealed in a glass capillary under an inert argon atmosphere. X-ray diffraction patterns were obtained at ambient conditions using a

Rigaku Rapid diffractometer employing Mo K $\alpha$  radiation and a curved area detector, with sample to detector distance refined using a high-purity silicon standard.

*In situ* DAC studies were performed at HPCAT, sector 16, Advanced Photon Source. Angular dispersive X-ray diffraction patterns were obtained with a wavelength of  $\lambda = 0.6199$  Å and a MAR image plate calibrated with a CeO<sub>2</sub> standard. The patterns were integrated using FIT2D software.<sup>29</sup>

*In situ* multianvil diffraction patterns were obtained at beamline ID06 of the European Synchrotron Radiation Facility (ESRF). Angular dispersive X-ray diffraction patterns were collected with a wavelength of  $\lambda = 0.3874$  Å and a scintillation counter served as the detector. The system was calibrated using a LaB<sub>6</sub> standard.

*In situ* measurements in PE cell were performed at beamline PSICHÉ of the SOLEIL synchrotron. The phase transformations were primarily observed by energy-dispersive X-ray diffraction ( $2\theta = 8^\circ$ ). After the crystallization of new phase, CAESAR system<sup>30</sup> was used to collect the data and consisted of energy-angle diagrams permitting identification of new structures and removal of artifacts. Several energies ( $\Delta E/E < 5\%$ ) were binned to obtain high-resolution angle-dispersive data. The system was calibrated using an Au standard.

Phase recognition and indexing of diffraction patterns was performed using PowderCell<sup>31</sup> and CheckCell.<sup>32</sup> Full profile Rietveld and Le Bail analyses were performed using GSAS<sup>33</sup> with EXPGUI.<sup>34</sup>

**Mass Spectrometry.** Recovered samples synthesized in multianvil runs were sealed in an evacuated glass tube with a septum. A few droplets of deionized water were introduced into the tube via syringe, and the resulting off-gases were sampled using a gastight syringe and analyzed using an Agilent 5890 gas chromatograph run isothermally ( $T = 35$  °C) equipped with a 30 m Agilent J&W GS-Carbonplot column interfaced to a 5972 quadrupole mass analyzer.

**NMR.** All solid state NMR experiments were run on a Chemagnetics Infinity Solid State NMR system. The static field of this instrument is 7.05 T yielding Larmor frequency for <sup>13</sup>C of 75 MHz. Direct polarization with magic angle spinning ( $\omega_1/2\pi = 11$  kHz) was employed using 5 mm inner diameter zirconia rotors and a doubly tuned MAS RF probe. Boron nitride inserts were employed around the sample to negate <sup>13</sup>C background from within the rotor. As the amount of sample was very small the issue of background signal from Vespel components of the stator in proximity to the RF coil is significant. In order to suppress the external background signal the 4 pulse DEPTH sequence run in a 16 pulse cycle suppresses any signal from nuclei that experience nutation less than 45°, when the sample nuclei experience RF induced nutation of 90°. The DEPTH sequence was applied for <sup>13</sup>C, where the 90° pulse lengths were 4  $\mu\text{s}$  for either nucleus. In the case of the <sup>13</sup>C DPMAS experiments, high-power <sup>1</sup>H–<sup>13</sup>C decoupling was applied with continuous irradiation ( $\omega_1/2\pi = 62.5$  kHz). For <sup>13</sup>C DPMAS NMR a recycle delay of 100 s was sufficient to avoid  $T_1$  saturation; note that a recycle delay of 10 s indicated  $T_1$  saturation. The number of acquisitions for <sup>13</sup>C DPMAS NMR was 1600. The spectral widths for <sup>13</sup>C DPMAS MNR were 50 and 200 kHz, respectively. All spectra were referenced to <sup>13</sup>C of tetramethylsilane (TMS).

**Raman Spectroscopy.** Raman spectra were obtained using a Princeton Instruments spectrograph (SP2750) with 750 mm focal length. A 532 nm diode laser was focused on the sample through a 20 $\times$  long working distance objective lens. Raman light was collected in the backscatter geometry, focused onto a 50  $\mu\text{m}$  entrance slit, and dispersed off of an 1800 grooves/mm grating onto a liquid-nitrogen-cooled charge-coupled device detector. The spectrometer was calibrated using the emission lines from a neon lamp.

**Ab Initio Calculations.** The structural searching algorithm USPEX,<sup>35</sup> coupled with density functional theory (DFT),<sup>36</sup> was used to determine new stable structures and to elucidate thermodynamic stability. Enthalpy calculations and geometry optimizations were performed within the framework of the generalized gradient approximation (GGA) with the Perdew–Burke–Ernzerhof (PBE) parametrization<sup>37</sup> for the exchange–correlation functional as implemented in VASP code. For Brillouin zone integration, we used the Monkhorst–Pack scheme<sup>38</sup> and checked convergence of ground state

calculations with uniformly increasing  $k$ -point meshes for each structure. We used a plane-wave basis-set cutoff of 500 eV and generated a  $12 \times 12 \times 12$   $k$ -point grid meshed for a Brillouin-zone integration.<sup>39</sup> Calculations of phonons of  $\text{Mg}_2\text{C}_3$  were performed with density functional perturbation theory as implemented in Quantum Espresso<sup>40</sup> code, and used a uniform  $4 \times 4 \times 4$   $q$ -mesh and dynamical matrix interpolation technique.

## RESULTS AND DISCUSSION

**Initial Observations.** The first observations of a new compound in the Mg–C system were made using LH-DACs with synchrotron PXRD. A sample of Mg–gC ( $x_{\text{C}} \approx 0.5$ ) was heated at 18 GPa to  $1750 \pm 250$  K, and quenched to ambient temperature for diffraction measurements. In addition to the formation of  $\text{Mg}_2\text{C}$ ,<sup>9</sup> several new reflections (Figure 1) were

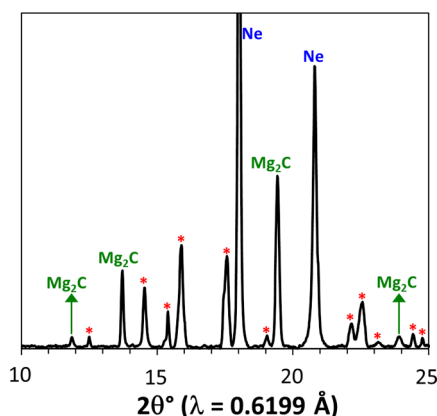


**Figure 1.** Synchrotron PXRD ( $\lambda = 0.6199$  Å) pattern recorded at 18 GPa showing typical multiphase synthesis obtained in the diamond anvil cell (DAC). The sample was heated at  $1750 \pm 250$  K.  $\text{Mg}_2\text{C}$  and Ne reflections are labeled. Asterisks indicate unidentified reflections, shown later to originate from  $\beta$ - $\text{Mg}_2\text{C}_3$ .

observed that could not be attributed to any known Mg–C structures. Given the limited number of observed reflections and the multiphase nature of synthesis, it was not possible to index these new lines with any appreciable degree of confidence.

Analogous PXRD patterns were obtained from samples recovered from MA runs at 9–15 GPa, 1770–2000 K, and  $0.33 \leq x_{\text{C}} \leq 0.93$ . Strong similarities between the *in situ* LH-DAC results and *ex situ* MA data suggest that the new structure is recoverable to ambient conditions, and is possible to synthesize over a broad range of  $p$ – $T$ – $x$  conditions. Like the LH-DAC data, it was not possible to solve the structure from laboratory PXRD results obtained from recovered MA samples.

**Mass Spectrometry and NMR.** In order to establish additional insights into the state of carbon within the new phase(s) recovered from MA experiments, the hydrolysis products of recovered samples were analyzed using mass spectrometry. A typical mass spectrum from a run at 9 GPa and 1770 K (outside of the formation region of  $\text{Mg}_2\text{C}$ ) is presented as Figure 2a. Aside from argon (from the glovebox) and constituents in air introduced during sample injection, propadiene and propyne,  $\text{C}_3\text{H}_4$ , were the only hydrolysis products detected in the mass spectrum. As for the case of previous reports of magnesium carbides synthesized at ambient pressure,<sup>15,16,41</sup> this observation provides strong chemical support that the new carbide phase contains  $[\text{C}=\text{C}=\text{C}]^{4-}$

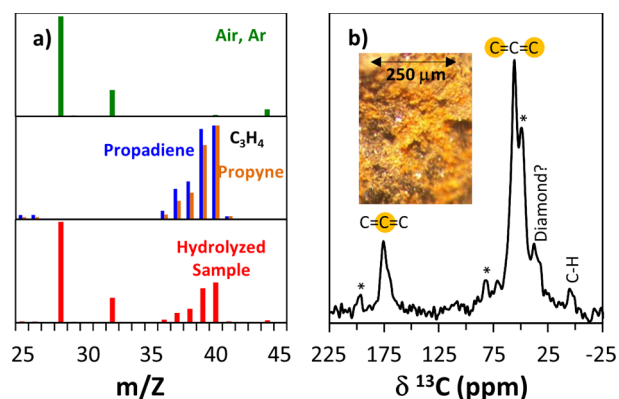


**Figure 2.** (a) Mass spectrum of the hydrolysis products of magnesium carbide synthesized at 9 GPa and 1770 K ( $x_{\text{C}} = 0.85$ ) compared with air and  $\text{C}_3\text{H}_4$ . (b)  $^{13}\text{C}$  MAS NMR spectrum. Asterisks indicate unidentified peaks which may originate from the multiphase nature of synthesis or possible presence of  $J$ -coupling. Inset shows image of the recovered sample.

anions and is likely a high-pressure polymorph of magnesium sesquicarbide,  $\text{Mg}_2\text{C}_3$ .

An MA synthesis experiment using  $^{13}\text{C}$  amorphous carbon (99% of isotope purity) was performed at 9 GPa and 1700 K (outside of the formation region of  $\text{Mg}_2\text{C}$ ) to further investigate the states of carbon in the new phase using  $^{13}\text{C}$  NMR (Figure 2b). While multiple peaks exist in the spectrum due to multiphase synthesis, two clear groupings occur near  $\delta = 50$  and 175 ppm, in an approximate 2:1 ratio. These resonances may be compared with pure allene, which displays shifts at  $\delta = 75$  and 213 ppm, originating from the end and central carbons of the three-carbon chains, respectively.<sup>42</sup> These observations are consistent with the presence of an allenide-type carbide, where the resonances are shifted upfield from the case of pure  $\text{C}_3\text{H}_4$ . These results are similar to other  $\text{C}_3^{4-}$  carbides including  $\text{Ca}_3\text{Cl}_2\text{C}_3$ , which shows resonances at 122 and 173 ppm,<sup>43</sup> and  $\text{LiCa}_2\text{C}_3\text{H}$ , which has resonances at 126 and 225 ppm in an approximate 2:1 ratio.<sup>44</sup> Thus, the NMR results are consistent with mass spectrometry in regards to the formation of an allenide-type carbide.

**Ab Initio Structural Predictions.** In order to help resolve the structure of the new Mg carbide phase, we performed pressure-dependent *ab initio* structural evolution searches based on density functional theory (DFT). The composition during the search was fixed to  $\text{Mg}_2\text{C}_3$ , as indicated by mass spectrometry and  $^{13}\text{C}$  NMR analyses. We performed the searching with up to 6 formula units in the simulation cell at pressures up to 20 GPa in 5 GPa increments. *Ab initio* structural evolution algorithms (USPEX method/code)<sup>35</sup> have demonstrated their power for the prediction of new high-pressure phases, and for elucidating structural solutions for complex experimental data. This method was previously shown to be powerful for complicated low-symmetry structures, such as orthorhombic boron<sup>45</sup> and unexpected sodium chlorides<sup>46</sup> and has become a more and more widely used technique.<sup>47,48</sup>

Figure 3a compares the pressure dependence of the relative enthalpies of the four lowest energy  $\text{Mg}_2\text{C}_3$  structures predicted by USPEX. The known  $\alpha$ - $\text{Mg}_2\text{C}_3$  ( $Pnmm$ ) structure was predicted to be the most stable at ambient pressure. With increasing pressure, a new monoclinic phase ( $C2/m$ ), unrelated by subgroup symmetry, becomes the most stable structure above 5 GPa and continues to gain enthalpic advantage, relative

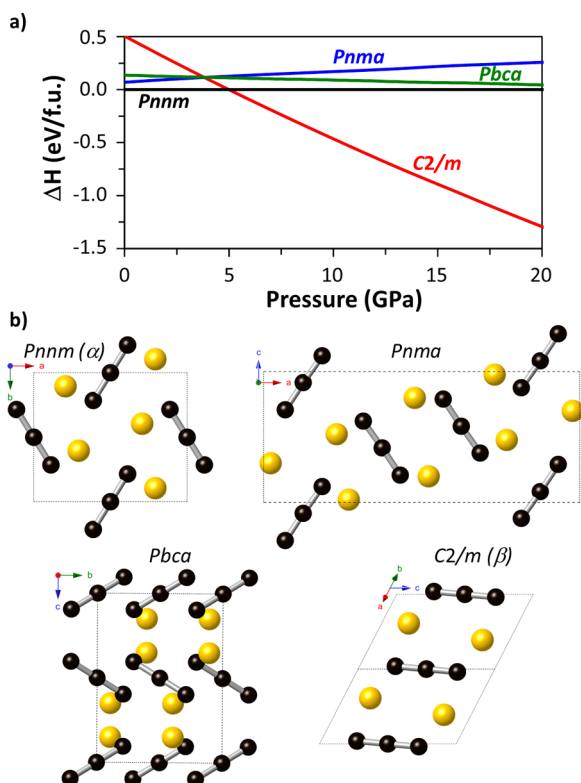


**Figure 3.** (a) Enthalpies of most stable  $\text{Mg}_2\text{C}_3$  polymorphs predicted by USPEX as a function of pressure, and (b) their structures.

to other structures, to at least 20 GPa. Two additional orthorhombic structures, with symmetries  $Pnma$  and  $Pbca$ , were also predicted to be within 0.25 eV/formula unit (f.u.), but do not become enthalpically stabilized relative to the  $Pnmm$  structure up to 20 GPa. The corresponding crystal structures of the most stable compounds with composition  $\text{Mg}_2\text{C}_3$  are presented in Figure 3b.

The predicted  $Pnma$  polymorph is quite similar to  $\alpha\text{-Mg}_2\text{C}_3$  ( $Pnmm$ ) and may be viewed roughly as the same structure with a doubling of the unit cell along the  $a$ -axis. One can see that the two polymorphs differ by the mutual organization of anionic  $[\text{C}=\text{C}=\text{C}]^{4-}$  layers: ABAB in the  $\alpha$ -phase and AABBAABB in  $Pnma$  phase. The linear chains in different layers are canted with respect to one another by an angle of  $\sim 70^\circ$  in both phases.

Like the other  $\text{Mg}_2\text{C}_3$  phases, the predicted monoclinic  $C2/m$  structure contains linear  $\text{C}_3^{4-}$  chains that are isoelectronic with  $\text{CO}_2$ . However, the mutual organization of anionic layers within the  $C2/m$  structure is completely different as compared with the orthorhombic structures: the  $[\text{C}=\text{C}=\text{C}]^{4-}$  chains are all oriented approximately along the  $c$ -direction. We speculate that this parallel orientation found in  $C2/m$  allows for more efficient packing of the linear carbon chains, which provides the physical basis for the enthalpic stabilization of this structure with increased pressure. Indeed, the volume per f.u. for the  $C2/m$  structure was calculated to be 8% smaller than that for the  $Pnmm$  structure at the transition pressure of 5 GPa. Crystallographic information for the lowest energy structures calculated for  $\text{Mg}_2\text{C}_3$  is provided in Table 1.

The calculated C=C bond lengths are similar for all three structures, ranging from 1.315 to 1.336 Å. The calculated C=C length for the  $Pnmm$  ( $\alpha$ ) structure of 1.315 Å agrees favorably with the experimental value of 1.332 Å reported previously.<sup>5</sup> The calculated length is slightly enhanced within the  $C2/m$  ( $\beta$ )

**Table 1.** Crystallographic Information for Low-Energy  $\text{Mg}_2\text{C}_3$  Polymorphs at Ambient Pressure

structure	lattice params	atomic coordinates
$Pnmm$ (No. 58)	$a = 6.168 \text{ \AA}$ $b = 5.204 \text{ \AA}$ $c = 3.428 \text{ \AA}$	C1@2d (0, 0.5, 0.5) C2@4g (0.388, 0.215, 0) Mg1@4g (0.793, 0.895, 0.5)
$C2/m$ (No. 12)	$a = 4.833 \text{ \AA}$ $b = 4.698 \text{ \AA}$ $c = 6.047 \text{ \AA}$	C1@2c (0, 0, 0.5) C2@4i (0.962, 0, 0.263) Mg1@4i (0.389, 0, 0.199)
	$\beta = 126.43^\circ$	
$Pnma$ (No. 62)	$a = 12.851 \text{ \AA}$ $b = 3.782 \text{ \AA}$ $c = 5.320 \text{ \AA}$	C1@4c (0.932, 0.250, 0.291) C2@4c (0.815, 0.250, 0.878) C3@4c (0.125, 0.750, 0.917) Mg1@4c (0.231, 0.750, 0.522) Mg2@4c (0.478, 0.250, 0.800)
$Pbca$ (No. 61)	$a = 6.230 \text{ \AA}$ $b = 5.200 \text{ \AA}$ $c = 7.024 \text{ \AA}$	C1@4a (0, 0, 0) C2@8c (0.551, 0.291, 0.096) Mg1@8c (0.117, 0.893, 0.350)

structure (1.332 Å), which may be caused by changes in  $\pi$  interaction with Mg. While the  $Pnmm$  structure has shorter Mg—C nearest neighbor contacts,  $\text{C}_3^{4-}$  units within the  $C2/m$  structure are coordinated by 10 Mg nearest neighbors, while  $\text{C}_3^{4-}$  units within  $Pnmm$  are coordinated by only eight (Figure 4).

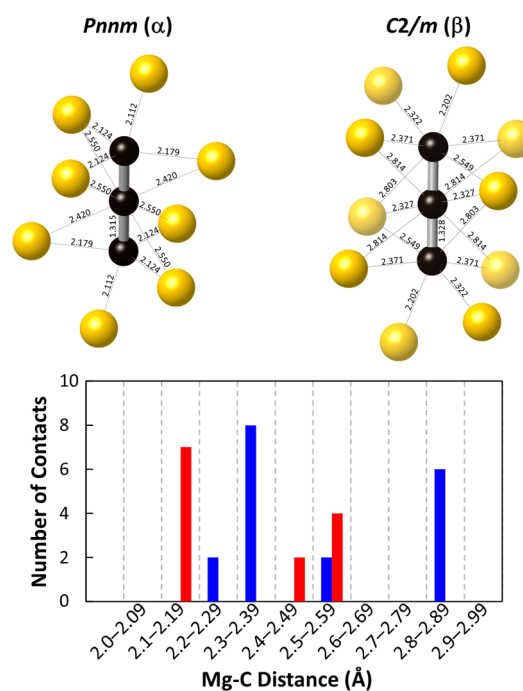


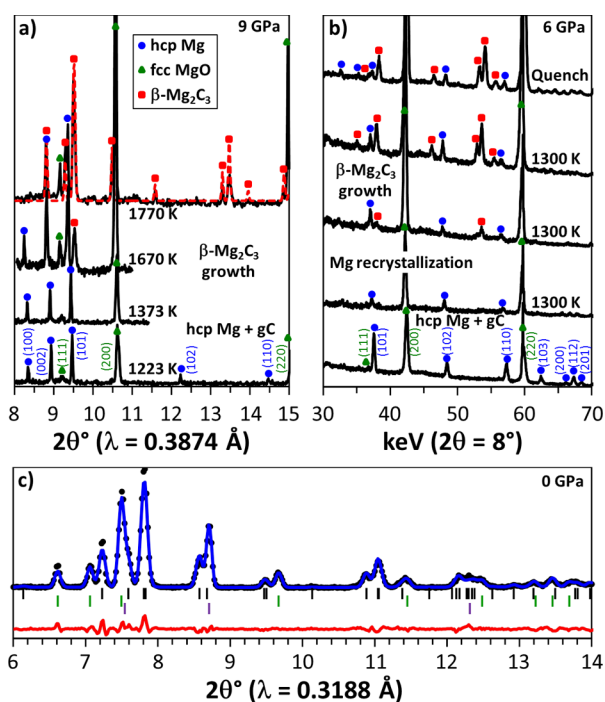
**Figure 4.**  $\text{C}_3^{4-}$  coordination in  $\alpha$  and  $\beta$   $\text{Mg}_2\text{C}_3$  and histogram of nearest neighbor Mg—C distances out to 3 Å.

Like  $\alpha\text{-Mg}_2\text{C}_3$ , the new monoclinic  $\beta$  phase is an indirect band gap semiconductor. Using DFT (PBE), we calculate the band gaps to be 1.23 and 1.69 eV for the  $\alpha$  and  $\beta$  phases, respectively. Using the HSE06 hybrid functional for exchange correlation,<sup>49</sup> which has been shown to produce more accurate band gaps than PBE, the gaps of the  $\alpha$  and  $\beta$  phases are 2.09 and 2.52 eV, respectively. The wide band gap of  $\beta\text{-Mg}_2\text{C}_3$  likely

contributes to the orangish color observed experimentally (Figure 2b).

**In Situ Synthesis of Pure  $\beta$ -Mg<sub>2</sub>C<sub>3</sub> (C2/m).** In order to overcome the challenges associated with multiphase synthesis in the DAC and recovered MA samples, we performed synthesis experiments in both MA (9 GPa) and PE presses (6.5 GPa), both with *in situ* synchrotron PXRD. In both cases, the homogeneous fixed starting compositions and uniform sample heating, combined with the ability to probe the structure under *in situ* conditions without additional handling requirements, allowed for the nearly phase-pure synthesis of the new carbide phase to be tested against the theoretical predictions.

During MA experiments performed at ID06 ESRF, new diffraction peaks were observed at the onset of Mg recrystallization at 9 GPa and  $\sim$ 1700 K ( $x_C = 0.33$ ). After approximately 1 h of heating at 1770 K, a series of new reflections were observed, which are in excellent agreement with the XRD pattern calculated for the newly predicted C2/m structure of Mg<sub>2</sub>C<sub>3</sub> (Figure 5a). The diffraction patterns



obtained under these conditions are completely described by this structure, combined with some excess Mg and MgO (used as a capsule material and pressure medium). Similarly, the new C2/m structure was also observed during *in situ* PE cell experiments at SOLEIL at 6 GPa ( $x_C = 0.5$ ). In this case, formation of the new phase also began during Mg recrystallization (1300 K), and was the only carbide phase

formed (MgO capsule and excess Mg were the only other phases observed) (Figure 5b).

The sample produced in the PE press at 6 GPa was decompressed to ambient pressure, and no phase transformations were observed, consistent with recoverability, and high-resolution angular dispersive data were collected (Figure 5c). Rietveld analysis of the synchrotron data confirms that this phase is indeed the predicted C2/m structure, with remarkable agreement between experiment and theory: the DFT lattice constants listed in Table 1 are all well within a one percent difference from the experimental lattice constants of  $a = 4.831(1)$  Å,  $b = 4.700(1)$  Å,  $c = 6.029(1)$  Å, and  $\beta = 126.71(1)^\circ$ . Thus, we have successfully identified the second known polymorph of magnesium sesquicarbide,  $\beta$ -Mg<sub>2</sub>C<sub>3</sub>.

**DAC Data and Equation of State.** With the structural solution of the monoclinic  $\beta$ -Mg<sub>2</sub>C<sub>3</sub> phase known, it was possible to revisit synchrotron XRD data sets from DAC runs that contained multiple carbide phases, e.g., Figure 1. These patterns, which contained on the order of 10 reflections from the monoclinic structure, were indexed as a function of pressure (Figure 6), and experimental lattice parameters show excellent

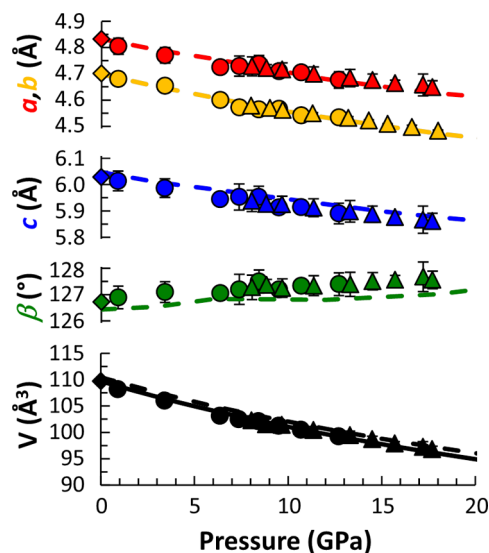


Figure 6. Lattice parameters and unit cell volume for  $\beta$ -Mg<sub>2</sub>C<sub>3</sub> with pressure. Dashed lines represent DFT calculations.

agreement with those obtained from DFT calculations. The lattice parameters  $a$ ,  $b$ , and  $c$  display a monotonically decreasing trend with pressure, while the monoclinic angle,  $\beta$ , increases slightly ( $<1\%$ ) between 0 and 20 GPa.

The  $p$ - $V$  data for Mg<sub>2</sub>C<sub>3</sub> were fit with a second-order Birch–Murnaghan equation of state with  $V_0 = 109.73(2)$  Å<sup>3</sup> and  $B_0 = 103(2)$  GPa ( $B_0' = 4$ , implied). These parameters are in good agreement with the DFT calculations where  $V_0 = 110.5$  Å<sup>3</sup>,  $B_0 = 106.5$  GPa, and  $B_0' = 4.2$ .  $\beta$ -Mg<sub>2</sub>C<sub>3</sub> is less compressible than acetylide-type alkali and alkaline earth metal carbides (e.g.,  $B_0 = 55$  GPa<sup>50</sup> for CaC<sub>2</sub>,  $B_0 = 49$  GPa<sup>51</sup> for BaC<sub>2</sub>), but is quite comparable to Mg<sub>2</sub>C ( $B_0 = 87(1)$  GPa<sup>9</sup>).

**Thermodynamic Stability of  $\beta$ -Mg<sub>2</sub>C<sub>3</sub>.** At ambient pressure, the previously known  $\alpha$ -phase of Mg<sub>2</sub>C<sub>3</sub> is metastable with respect to its formation components by  $\Delta H_f^\circ = +79.5$  kJ/mol,<sup>11</sup> yet its synthesis is indeed possible through various chemical routes.<sup>5,10,15</sup> With increasing pressure, the formation enthalpy of  $\alpha$ -Mg<sub>2</sub>C<sub>3</sub> decreases, but this structure never

becomes thermodynamically stabilized up to 20 GPa, according to our zero-temperature DFT calculations (Figure 7).

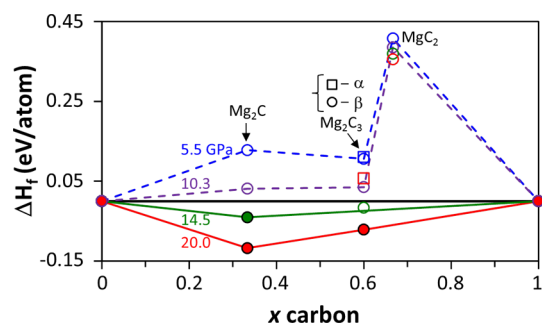


**Figure 7.** Convex hull of formation enthalpies for Mg–C with respect to hcp Mg and graphite as a function of pressure at 0 K. Thermodynamically stable phases (filled symbols) are connected by solid lines, while metastable phases (open symbols) are connected by dashed lines. Two points (5.5 and 20 GPa) are provided for  $\alpha$ -Mg<sub>2</sub>C<sub>3</sub>, indicated by the open squares.  $\beta$ -Mg<sub>2</sub>C<sub>3</sub> becomes a stable structure on the convex hull above 19 GPa. The  $P4_3/mnm$  structure was used for MgC<sub>2</sub>.<sup>8</sup>

Above 5 GPa,  $\beta$ -Mg<sub>2</sub>C<sub>3</sub> becomes more stable than the  $\alpha$ -phase, but still remains metastable with respect to a mixture of hcp Mg and graphite. Above 13 GPa  $\beta$ -Mg<sub>2</sub>C<sub>3</sub> achieves a negative enthalpy of formation, but thermodynamic stability is not achieved due to disproportionation into Mg<sub>2</sub>C and graphite. It is not until pressures above 19 GPa that  $\beta$ -Mg<sub>2</sub>C<sub>3</sub> becomes a stable structure on the convex hull. These calculations are qualitatively consistent with experimental observations; however, observations differ substantially in terms of absolute pressure. At 5 GPa and below no formation of any carbide was observed in experiments: after the disappearance of Mg diffraction lines, neither long heating (up to 1–2 h) nor temperature increase led to appearance of new reflections in diffraction patterns, while in the recovered samples only metallic Mg and partially ordered graphite were observed. This agrees with calculations in terms of low-pressure thermodynamic instability. However, during experiments at 6 GPa and above, we clearly observed the formation of  $\beta$ -Mg<sub>2</sub>C<sub>3</sub> directly from a mixture of formation elements. Under *in situ* experiments this formation occurs at the point of Mg recrystallization. According to calculations,  $\beta$ -Mg<sub>2</sub>C<sub>3</sub> should still be thermodynamically metastable at pressures below 19 GPa; however, nonzero temperature effects likely explain this apparent discrepancy. Kinetic pathways accessible by experiment might also contribute to  $\beta$ -Mg<sub>2</sub>C<sub>3</sub> formation at reduced pressure as compared with calculations, although this effect is likely minimal compared with the effect of temperature. Below 11 GPa, Mg<sub>2</sub>C clearly decomposes into  $\beta$ -Mg<sub>2</sub>C<sub>3</sub> + C during isothermal decompression at 1550 K.<sup>21</sup> The formation of  $\beta$ -Mg<sub>2</sub>C<sub>3</sub> through two entirely independent  $p$ - $T$ - $x$  pathways (direct reaction with the elements and Mg<sub>2</sub>C decomposition) indicates thermodynamic stability at finite temperature.

While thermodynamically metastable at 0 GPa, the experimentally observed ambient pressure recoverability of  $\beta$ -Mg<sub>2</sub>C<sub>3</sub> is also supported by density functional perturbation theory calculations. The absence of imaginary vibrational frequencies in phonon dispersion relations calculated at ambient pressure (Figure 8) indicates that  $\beta$ -Mg<sub>2</sub>C<sub>3</sub> is dynamically stable at 0 GPa.

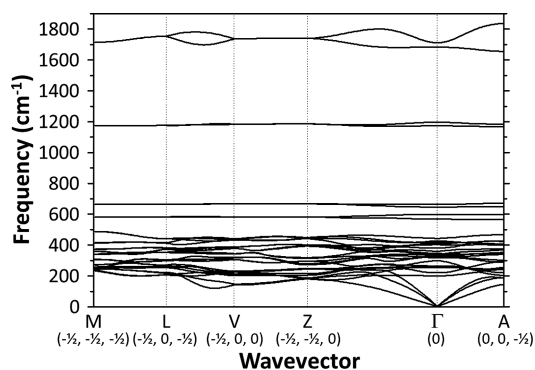


**Figure 8.** Phonon dispersion relations of  $\beta$ -Mg<sub>2</sub>C<sub>3</sub> at ambient pressure.

**Raman Spectra of  $\beta$ -Mg<sub>2</sub>C<sub>3</sub>.** Raman spectra of  $\beta$ -Mg<sub>2</sub>C<sub>3</sub> were recorded at room temperature as a function of pressure for samples synthesized between 15 and 20 GPa and 1700–2000 K in LH-DACs (Figure 9). Symmetry analysis of the C<sub>2</sub>/

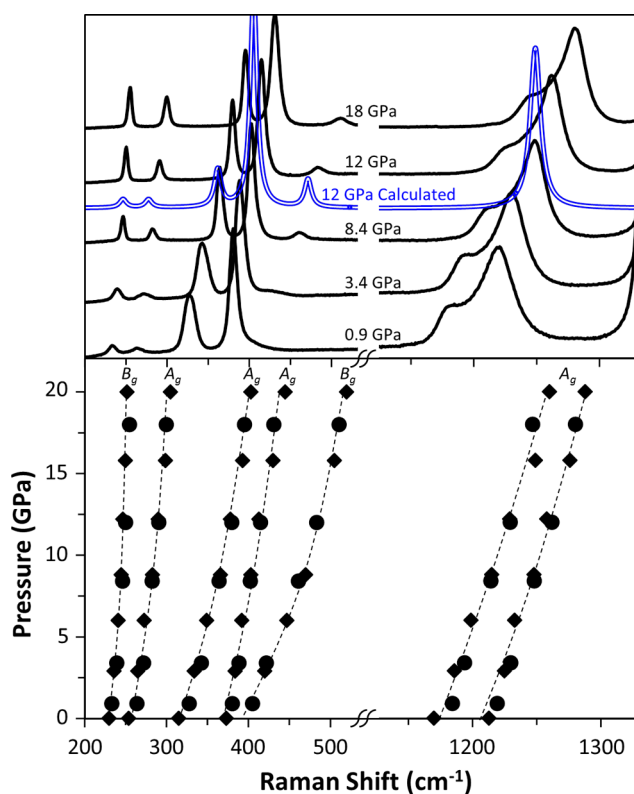


**Figure 9.** Raman spectra of  $\beta$ -Mg<sub>2</sub>C<sub>3</sub> with pressure (top) and observed frequencies (bottom). Calculated Raman intensities at 12 GPa, represented by Lorentzian peaks, are shown in the top panel as a double line. Dashed lines in the bottom panel guide the eye. All Raman active modes have A<sub>g</sub> or B<sub>g</sub> representations.

*m* structure reveals 4A<sub>g</sub> + 2B<sub>g</sub> Raman active modes for  $\beta$ -Mg<sub>2</sub>C<sub>3</sub>. All modes were observed experimentally, and all displayed positive frequency correlation with pressure. The mode observed at 1213 cm<sup>-1</sup> (0 GPa) is assigned to C=C stretching and clearly confirms the presence of the allylenide anion. Normal mode analysis of phonon dispersion relations at the  $\Gamma$  point reveals this mode to be associated with symmetric stretching (A<sub>g</sub>). Experimentally, this mode was observed as a doublet with a second feature at 1170 cm<sup>-1</sup>, which might originate from a subtle distortion of the monoclinic cell. The

calculated optical phonon branch (Figure 8) does indeed show two modes at 1171 and 1192  $\text{cm}^{-1}$ ; however, the lower frequency mode is not Raman active in the undistorted  $C2/m$  structure. Asymmetric stretching modes, calculated to occur at 1683 and 1711  $\text{cm}^{-1}$ , are not Raman active, but the mode at 1711  $\text{cm}^{-1}$  was calculated to have strong IR intensity. The stretching modes in  $\beta\text{-Mg}_2\text{C}_3$  agree favorably with those for  $\text{Ca}_3\text{C}_3\text{Cl}_2$  ( $\nu_{\text{sym}} = 1159 \text{ cm}^{-1}$ ,  $\nu_{\text{asym}} = 1660 \text{ cm}^{-1}$ ), a structure previously reported to contain the  $\text{C}_3^{4-}$  anion.<sup>52</sup> The only other structure containing  $\text{C}_3^{4-}$  with vibrational spectroscopy data available,  $\text{Ca}_{11}\text{Sn}_3\text{C}_8$ , exhibits stretching modes at  $\nu_{\text{sym}} = 968 \text{ cm}^{-1}$ ,  $\nu_{\text{asym}} = 1482, 1542 \text{ cm}^{-1}$ .

The five remaining modes originate from librational-like motion of the  $[\text{C}=\text{C}=\text{C}]^{4-}$  anions. Bending modes near 600  $\text{cm}^{-1}$  are not Raman active for the  $C2/m$  structure, but are calculated to have appreciable IR intensity. Our calculated Raman frequencies for  $\text{Mg}_2\text{C}_3$  at 12 GPa agree very well with experiment showing an average deviation of only  $-2.5\%$ , and the calculated relative intensities are also in general agreement with experiment.

## CONCLUSIONS

After exploring pressure as additional dimension for chemistry of the Mg–C system, four magnesium carbides are now known: (1) tetragonal  $\text{MgC}_2$ , (2) orthorhombic  $\alpha\text{-Mg}_2\text{C}_3$ , (3) monoclinic  $\beta\text{-Mg}_2\text{C}_3$ , and (4) cubic  $\text{Mg}_2\text{C}$ . Taking into account that at ambient pressure and at pressures up to  $\sim 5$  GPa the elements do not interact at any temperature, it is quite astonishing to observe such rich chemistry: two metastable carbides accessible by chemical routes (cases 1–2), different organization of  $\text{C}_3^{4-}$  linear chains as a function of pressure and temperature (cases 2–3), as well as stabilization of the unusual  $\text{C}^{4-}$  anion at pressures of 15 GPa and higher (case 4). Although these compounds are strongly ionic, they remain metastable at ambient conditions after recovery from high pressure, an atypical situation for ionic compounds of nontransition metals, which usually easily pass into stable structures upon decompression without hysteresis, even at low temperatures.

## AUTHOR INFORMATION

### Corresponding Author

\*E-mail: tstrobel@ciw.edu.

### Author Contributions

The manuscript was written through contributions of all authors. All authors have given approval to the final version of the manuscript.

### Funding

This work was supported by DARPA under ARO Contracts W31P4Q-13-1-005, W911NF-11-1-0300, and W31P4Q-12-1-008. D.Y.K. was supported by the Energy Frontier Research in Extreme Environments Center (EFREE) under Award DE-SG0001057. Portions of this work were performed at HPCAT (Sector 16), Advanced Photon Source (APS), Argonne National Laboratory. HPCAT operations are supported by DOE-NNSA under Award DE-NA0001974 and DOE-BES under Award DE-FG02-99ER45775, with partial instrumentation funding by NSF. APS is supported by DOE-BES, under Contract DE-AC02-06CH11357.

### Notes

The authors declare no competing financial interest.

## ACKNOWLEDGMENTS

We thank D. Foustoukos for help with mass spectrometry measurements, A. Karandikar and R. Boehler for assistance with preliminary laser heating experiments, and Y. Meng for assistance with synchrotron XRD measurements. The *in situ* experiments on high-pressure synthesis were performed on the ID06 beamline at the European Synchrotron Radiation Facility (ESRF), Grenoble, France, with beamtime allocated to Proposal CH-3601. We also acknowledge SOLEIL for provision of synchrotron radiation facilities (Proposal 20130222), and we would like to thank K. Cherednechenko and J.-P. Itié for assistance in using beamline PSICHÉ.

## ABBREVIATIONS

HP, high pressure; HT, high temperature; PXRD, powder X-ray diffraction; NMR, nuclear magnetic resonance

## REFERENCES

- (1) Ruschewitz, U. *Coord. Chem. Rev.* **2003**, *244*, 115.
- (2) von Stackelberg, M. *Z. Phys. Chem. B* **1930**, *9*, 437.
- (3) Juza, R.; Wehle, V.; Schuster, H. U. *Z. Anorg. Allg. Chem.* **1967**, *352*, 252.
- (4) Von Stackelberg, M.; Quatram, F. *Z. Phys. Chem.* **1935**, *27*, 50.
- (5) Fjellvag, H.; Karen, P. *Inorg. Chem.* **1992**, *31*, 3260.
- (6) Pottgen, R.; Jeitschko, W. *Inorg. Chem.* **1991**, *30*, 427.
- (7) Hoffmann, R.; Meyer, H. J. *Z. Anorg. Allg. Chem.* **1992**, *607*, 57.
- (8) Karen, P.; Kjekshus, A.; Huang, Q.; Karen, V. L. *J. Alloy. Compd.* **1999**, *282*, 72.
- (9) Kurakevych, O. O.; Strobel, T. A.; Kim, D. Y.; Cody, G. D. *Angew. Chem., Int. Ed.* **2013**, *52*, 8930.
- (10) Novak, J. *Z. Phys. Chem.* **1910**, *73*, 513.
- (11) Chase, M. W. *J. Phys. Chem. Ref. Data* **1998**, *9*, 1 monograph.
- (12) Irmann, F. *Helv. Chim. Acta* **1948**, *31*, 1584.
- (13) Hajek, B.; Karen, P.; Brozek, V. *Collect. Czech. Chem. Commun.* **1983**, *48*, 1969.
- (14) Hajek, B.; Karen, P.; Brozek, V. *Collect. Czech. Chem. Commun.* **1983**, *48*, 1963.
- (15) Hajek, B.; Karen, P.; Brozek, V. *Collect. Czech. Chem. Commun.* **1980**, *45*, 3408.
- (16) Cordes, J. F.; Wintersberger, K. *Z. Naturforsch., B* **1957**, *12*, 136.
- (17) Vohn, V.; Ruschewitz, U. *Z. Kristallogr. Suppl.* **1998**, *15*, 55.
- (18) Srepusharwoot, P.; Blomqvist, A.; Araujo, C. M.; Scheicher, R. H.; Ahuja, R. *Phys. Rev. B* **2010**, *82*, 125439.
- (19) Karttunen, A. J.; Fassler, T. F.; Linnolahti, M.; Pakkanen, T. A. *Inorg. Chem.* **2011**, *50*, 1733.
- (20) Corkill, J. L.; Cohen, M. L. *Phys. Rev. B* **1993**, *48*, 17138.
- (21) Kurakevych, O. O.; Le Godec, Y.; Strobel, T. A.; Kim, D. Y.; Crichton, W. A.; Guignard, J. *J. Phys. Chem. C* **2014**, *118*, 8128–8133.
- (22) Solozhenko, V. L.; Kurakevych, O. O.; Andraut, D.; Le Godec, Y.; Mezouar, M. *Phys. Rev. Lett.* **2009**, *102*, 015506.
- (23) Bertka, C. M.; Fei, Y. W. *J. Geophys. Res.: Solid Earth* **1997**, *102*, S251.
- (24) Errandonea, D.; Meng, Y.; Hausermann, D.; Uchida, T. *J. Phys.: Condens. Matter* **2003**, *15*, 1277.
- (25) Dorogokupets, P. I.; Dewaele, A. *High Pressure Res.* **2007**, *27*, 431.
- (26) Mao, H. K.; Xu, J.; Bell, P. M. *J. Geophys. Res.* **1986**, *91*, 4672.
- (27) Meng, Y.; Shen, G.; Mao, H. K. *J. Phys.: Condens. Matter* **2006**, *18*, S1097.
- (28) Makareno, I. *UPMC Internal Report*; 1995.
- (29) Hammersley, A. *ESRF Internal Report ESRF97HA02T*; 1997
- (30) Wang, Y. B.; Uchida, T.; Von Dreele, R.; Rivers, M. L.; Nishiyama, N.; Funakoshi, K.; Nozawa, A.; Kaneko, H. *J. Appl. Crystallogr.* **2004**, *37*, 947.
- (31) Kraus, W.; Nolze, G. *J. Appl. Crystallogr.* **1996**, *29*, 301.

- (32) Laugier, J.; Bochu, B. *LMGP-Suite Suite of Programs for the Interpretation of X-ray Experiments*; ENSP/Laboratoire des Matériaux et du Génie Physique: Saint Martin d'Hères, France.
- (33) Larson, A. C.; Von Dreele, R. B. *Los Alamos National Laboratory Report LAUR 86-748*; 1994.
- (34) Toby, B. H. *J. Appl. Crystallogr.* **2001**, *34*, 210.
- (35) Oganov, A. R.; Glass, C. W. *J. Chem. Phys.* **2006**, *124*, 244704.
- (36) Hohenberg, P.; Kohn, W. *Phys. Rev. B* **1964**, *136*, 864.
- (37) Perdew, J. P.; Chevary, J. A.; Vosko, S. H.; Jackson, K. A.; Pederson, M. R.; Singh, D. J.; Fiolhais, C. *Phys. Rev. B* **1992**, *46*, 6671.
- (38) Monkhorst, H. J.; Pack, J. D. *Phys. Rev. B* **1976**, *13*, 5188.
- (39) Baroni, S.; de Gironcol, S.; Dal Corso, A.; Giannozzi, P. *Rev. Mod. Phys.* **2001**, *73*, 515.
- (40) Giannozzi, P.; Baroni, S.; Bonini, N.; Calandra, M.; Car, R.; Cavazzoni, C.; Ceresoli, D.; Chiarotti, G. L.; Cococcioni, M.; Dabo, I.; Dal Corso, A.; de Gironcoli, S.; Fabris, S.; Fratesi, G.; Gebauer, R.; Gerstmann, U.; Gougousis, C.; Kokalj, A.; Lazzeri, M.; Martin-Samos, L.; Marzari, N.; Mauri, F.; Mazzarello, R.; Paolini, S.; Pasquarello, A.; Paulatto, L.; Sbraccia, C.; Scandolo, S.; Sclauzero, G.; Seitsonen, A. P.; Smogunov, A.; Umari, P.; Wentzcovitch, R. M. *J. Phys.: Condens. Matter* **2009**, *21*, 395502.
- (41) Disch, S.; Cheetham, A. K.; Ruschewitz, U. *Inorg. Chem.* **2008**, *47*, 969.
- (42) Beeler, A. J.; Orendt, A. M.; Grant, D. M.; Cutts, P. W.; Michl, J.; Zilm, K. W.; Downing, J. W.; Facelli, J. C.; Schindler, M. S.; Kutzelnigg, W. *J. Am. Chem. Soc.* **1984**, *106*, 7672.
- (43) Meyer, H. J. In *Inorganic Chemistry in Focus III*; Meyer, G., Naumann, D., Wesemann, L., Eds.; Wiley-VCH: New York, 2006; p 124.
- (44) Lang, D. A.; Zaikina, J. V.; Lovingood, D. D.; Gedris, T. E.; Lattner, S. E. *J. Am. Chem. Soc.* **2010**, *132*, 17523.
- (45) Oganov, A. R.; Chen, J.; Gatti, C.; Ma, Y.; Ma, Y.; Glass, C. W.; Liu, Z.; Yu, T.; Kurakevych, O. O.; Solozhenko, V. L. *Nature* **2009**, *460*, 292.
- (46) Zhang, W. W.; Oganov, A. R.; Goncharov, A. F.; Zhu, Q.; Bouffelfel, S. E.; Lyakhov, A. O.; Stavrou, E.; Somayazulu, M.; Prakapenka, V. B.; Konopkova, Z. *Science* **2013**, *342*, 1502.
- (47) Zhu, Q.; Oganov, A. R.; Glass, C. W.; Stokes, H. T. *Acta Crystallogr., Sect. B* **2012**, *68*, 215.
- (48) Oganov, A. R.; Lyakhov, A. O.; M, V. *Acc. Chem. Res.* **2011**, *44*, 227.
- (49) Krukau, A. V.; Vydrov, O. A.; Izmaylov, A. F.; Scuseria, G. E. *J. Chem. Phys.* **2006**, *125*, 224106.
- (50) Li, Y. L.; Luo, W.; Zeng, Z.; Lin, H. Q.; Mao, H. K.; Ahuja, R. *Proc. Natl. Acad. U.S.A.* **2013**, *110*, 9289.
- (51) Efthimiopoulos, I.; Kunc, K.; Vazhenin, G. V.; Stavrou, E.; Syassen, K.; Hanfland, M.; Liebig, S.; Ruschewitz, U. *Phys. Rev. B* **2012**, *85*, 054105.
- (52) Meyer, H. J. *Z. Anorg. Allg. Chem.* **1991**, *593*, 185.
- (53) Blankenship, T. V.; Lita, A.; Lattner, S. E. *Inorg. Chem.* **2012**, *51*, 13345.